Time-course studies by synchrotron X-ray solution scattering of the structure of human low-density lipoprotein during Cu^{2+}-induced oxidation in relation to changes in lipid composition

David F. MEYER*, Adam S. NEALIS*, Colin H. MacPHEE†, Pieter H. E. GROOT†, Keith E. SUCKLING†, K. Richard BRUCKDORFER* and Stephen J. PERKINS*‡

*Department of Biochemistry and Molecular Biology, Royal Free Hospital School of Medicine, Rowland Hill Street, London NW3 2PF, U.K., and †Department of Vascular Biology, SmithKline Beecham Pharmaceuticals Research and Development, The Frythe, Welwyn, Herts. AL6 9AR, U.K.

Low-density lipoproteins (LDLs) in plasma are constructed from a single molecule of apolipoprotein B-100 (apoB) (M_r 512000) in association with lipid [approximate M_r $(2–3) \times 10^6$]. LDL oxidation is an important process in the development of atherosclerosis, and can be imitated by the addition of Cu^{2+} ions. Synchrotron X-ray scattering of LDL yields curves without radiation damage effects at concentrations close to physiological. The radius of gyration R_G for preparations of LDL from different donors ranged between 12.1 and 16.0 nm, with a mean of 13.9 nm. At 4 °C, the distance distribution curve $P(r)$ indicated a maximum dimension of 25–27 nm for LDL, a peak at 19.5 nm which corresponds to a surface shell of protein and phospholipid head groups in LDL, and submaxima between 1.7 and 13.5 nm, which correspond to an ordered lipid core in LDL. LDL from different donors exhibited distinct $P(r)$ curves. For oxidation studies of LDL by X-rays, data are best obtained at 4 °C at a concentration of $\geqslant 2$ mg of LDL protein/ml together with controls based on non-oxidized LDL. LDL oxidation (2 mg of apoB/ml) was studied at 37 °C in the presence of 6.4, 25.6 and 51.2 μmol of Cu^{2+}/g of apoB. Large changes in $P(r)$ were reproducibly observed in the inter-particle distance range between 13 and 16 nm shortly after initiation of oxidation. This corresponds to the phospholipid hydrocarbon in LDL, which has either increased in electron density during oxidation or become increasingly disordered. After 25 h, the structural changes subsequently spread to regions of the $P(r)$ curves assigned to surface apoB and the central core of cholesteryl esters and triacylglycerols. Lipid analyses were carried out under the same solution conditions. The α-tocopherol and β-carotene antioxidant contents of LDL were consumed within 1–2 h. Analyses of the formation of thiobarbituric acid-reactive substances and lipid hydroperoxides indicated that arachidonic acid was preferentially oxidized before the maximal formation of lipid hydroperoxides at 8–12 h after initiation of oxidation. High-performance TLC showed that phosphatidylcholine was continuously converted into lysophosphatidylcholine during oxidation, which is consistent with the early changes in the X-ray $P(r)$ curves. The neutral core lipids became modified only after 12–15 h of oxidation. The combination of X-ray scattering structural analyses with biochemical analyses shows that the oxidation of LDL first affects the outer shell of surface phospholipid, then it spreads towards damage of apoB and the internal neutral lipid core of LDL.

INTRODUCTION

Low-density lipoproteins (LDLs) constitute a major family of cholesterol transporters in plasma [1]. LDLs are formed from single copies of apolipoprotein B-100 (apoB) mainly located on the surface, together with a phospholipid monolayer associated with free cholesterol, and a hydrophobic lipid core containing cholesteryl esters and to a lesser extent triacylglycerols. LDLs exist as a range of subfractions within and among individuals, and these may exhibit differences in biochemical properties [2,3]. Increased plasma levels of LDL correlate with the incidence of cardiovascular disease, which is a leading cause of death in the Western world [4,5]. There is now considerable evidence for the oxidation of LDL during the pathogenesis of atherosclerosis [5–8]. After oxidation, LDL becomes susceptible to uptake and internalization by scavenger receptors on macrophages. This leads to the formation of foam cells in the subendothelial space, and these are closely associated with the development of atherosclerotic plaques. Cellular oxidation of LDL *in vitro* can be mimicked by incubation with transition metals. The naturally occurring antioxidants in LDLs and plasma protect them from oxidation [7,9].

While the biochemical aspects of LDL oxidation have been studied in detail, fewer studies have been reported on the structural aspects of LDL oxidation. Large structural changes in LDL in terms of its self-aggregation are evident during oxidation, as detected by neutron scattering [10,11]. The joint use of neutron and X-ray solution scattering offers complementary but different views of the structure of LDL [12]. Neutron data on LDL in 100% ^2H_2O buffers monitor the external appearance of a polydisperse spherical structure of almost uniform scattering density [13]. X-ray scattering monitors the internal structure of LDLs in solution, since their lipid and protein components have different scattering densities which permits these to be readily distinguished from each other [14]. The maximum diameter of LDL was thus shown to be between 23 and 25 nm, and the internal structure contains a core of cholesteryl esters and triacylglycerols in two concentric shells surrounded by a surface monolayer of phospholipids, free cholesterol and protein [14]. Earlier X-ray work utilized unphysiologically high LDL concen-

Abbreviations used: LDL, low-density lipoprotein; ITP, indirect transformation procedure; HPTLC, high-performance TLC; apoB, apolipoprotein B-100 protein of LDL; TBARS, thiobarbituric acid-reactive substances.

‡ To whom correspondence and requests for reprints should be addressed.

trations, and the effect of LDL polydispersity on X-ray-scattering curves has not been characterized. New developments in synchrotron X-ray-scattering cameras [15,16] now permit the measurement within 10 min of the full scattering curve $I(Q)$ for dilute LDL samples with excellent signal-to-noise ratios. This makes possible the detailed study of native LDLs and the time-course study of internal structural changes in LDLs during oxidation.

Analyses of LDL oxidation by X-ray scattering require knowledge of both the structural properties of polydisperse LDL preparations as well as the events that occur during oxidation. Accordingly, X-ray data from a concentration series of native LDLs are presented, and the effect of LDL polydispersity on X-ray-scattering curves are assessed. This complements the analyses of native LDLs by neutron scattering [13]. Next, X-ray-scattering data for LDLs undergoing oxidation under the same conditions used in neutron oxidation studies [11] are presented. The X-ray data on LDL protein–lipid structures are supported by complementary investigations of the lipid composition of LDL in order to correlate the time course of internal structural change with changes in LDL lipid during oxidation. These investigated (i) the rate of depletion of antioxidants in LDLs, (ii) the rates of formation of lipid hydroperoxides and malondialdehyde from LDL lipids during lipid degradation, and (iii) the quantitative measurements of the amounts of polar and neutral lipids in LDLs and the changes in these during oxidation. This combination of X-ray scattering and compositional data shows that the outer shell of phospholipid hydrocarbons in LDLs is first affected by oxidative breakdown, and this is followed by structural changes involving apoB and the central core of neutral lipids (triacylglycerols and cholesteryl esters).

MATERIALS AND METHODS

Preparation of human LDLs for scattering and oxidation experiments

LDLs (density range 1.025–1.055 g/ml) were isolated by ultracentrifugation, and protein concentrations were determined as described previously [11,13]. LDLs were dialysed against 12.5 mM Tris/140 mM NaCl, pH 7.4, in water solvents for both X-ray scattering and biochemical experiments. LDL oxidation was initiated as before [11] within the week after LDL preparation. During oxidation, the Cu^{2+}-LDL samples (2 mg of apoB/ml) were incubated in Eppendorf vials at 37 °C in a water bath for up to 50 h at concentrations of Cu^{2+} ranging from 0 to 102.4 μM. Aliquots were removed by syringe and injected into the X-ray sample holder immediately prior to data acquisition or otherwise to biochemical assay. During the oxidation time course, samples were gently inverted in their vials to ensure the uniformity of oxidation conditions.

X-ray-scattering-data acquisition and reduction

Synchrotron X-ray data were obtained in six sessions on the scattering camera at Station 8.2 with a quadrant detector at the Synchrotron Radiation Source (SRS), Daresbury, U.K. [15,16]. The storage ring operated at 2.0 GeV with beam currents between 119 and 284 mA. Sample-to-detector distances were between 3.230 and 3.537 m. The detector Q range was calibrated using rat tail collagen, where $Q = 4\pi(\sin\theta)/\lambda$, where 2θ is the scattering angle and λ is the wavelength. Detector responses were measured using a ^{55}Fe source. Samples of thickness 1 mm were measured for 10 min at a temperature between 4 and 40 °C in Perspex cells with mica windows of thickness 10–15 μm. Time-frame analyses were used to check for the absence of radiation effects. Curves were normalized using an ionization chamber monitor reading between the sample and detector. Data analyses were performed using OTOKO software (P. Bendall, J. Bordas, M. H. C. Koch and G. R. Mant, EMBL Hamburg and Daresbury Laboratory, unpublished software). For native LDLs, 22 dilution series were measured (LDL protein between 0.9 and 10.9 mg/ml), based on 17 LDL samples from 12 donors (six male and six female, aged 20–45 years). For oxidized LDLs, data at 4 °C, or sometimes at 15 °C, were obtained at 6–13 time points for nine different LDL samples with up to four different Cu^{2+} concentrations of 0, 6.4, 25.6 and 51.2 μmol Cu^{2+}/g of apoB during a period of 50 h. Oxidation experiments used an apoB concentration of 2 mg/ml to avoid concentration effects. In an oxidation series, the same LDL sample was used for all Cu^{2+} concentrations as well as the blank without Cu^{2+} to avoid polydispersity effects.

Scattering-curve analyses

Guinier analyses of the scattering curves $I(Q)$ at low Q give the radius of gyration R_G and the forward scattering $I(0)$ [17] as:

$$\ln I(Q) = \ln I(0) - R_G^2 Q^2/3$$

For a spherical macromolecule, this is valid up to a $Q \cdot R_G$ of 1.3, and approximate in the $Q \cdot R_G$ range up to 2. For a given solute–solvent density-contrast difference, the R_G is a measure of both particle elongation and the internal arrangement of different scattering densities. $I(0)/c$ (c = sample concentration, defined by the LDL protein concentration) is proportional to the relative molecular mass M_r. The M_r is calculated as a relative value from X-ray data, normalized by the detector response.

Glatter's indirect transformation procedure (ITP) [17] (program versions ITP-81 and ITP-91) was used to transform $I(Q)$ into the electron-pair-distance-distribution function $P(r)$ in real space [14]:

$$P(r) = \frac{1}{2\pi^2}\int_0^\infty I(Q) Qr \sin(Qr) dQ$$

$P(r)$ corresponds to the distribution of distances r between any two volume elements within one particle weighted by the product of their respective electron densities relative to the solvent density. About 430 $I(Q)$ data points in the Q ranges 0.05–2.48 nm^{-1} or 0.04–2.21 nm^{-1} from the quadrant detector were funnelled to give 290–301 data points, normalized, and extrapolated to zero concentration. The $I(Q)$ curve was fitted using 20 splines, and transformed using a D_{max} of 30 nm after optimization using stability plots [18]. The minimum Q value required for ITP was determined to be 0.13 nm^{-1} from the stricter of the two relationships given in [18], namely $Q_{min} \cdot D_{max} \leqslant \pi$, where $D_{max} = 23$ nm. This is met by the camera on Station 8.2. Criteria for the correct choice of $P(r)$ transformation parameters were: (i) $P(r)$ should be zero when r is zero; (ii) the R_G and $I(0)$ values calculated from $P(r)$ should agree with those from the Guinier analyses; (iii) $P(r)$ should be stable and reproducible for different $I(Q)$ curves obtained under similar experimental conditions.

The X-ray $P(r)$ curves were converted using the program DECON-91 into the electron radial-density functions $\rho(r)$. This assumes that LDL is spherically symmetric and monodisperse (however, see below). The conversion corresponds to the Fourier transformation of the scattering amplitude $A(Q) = \pm\sqrt{I(Q)}$:

$$\rho(r) = \frac{1}{2\pi^2}\int_0^\infty A(Q) Q^2 \frac{\sin Qr}{Qr} dQ$$

The transformations used 20 radial electron-density steps, each of width 0.75 nm, based on an assumed LDL radius of 15 nm. Stabilization plots were used to optimize the transformation. Criteria for correctly calculated $\rho(r)$ curves were: (i) $\rho(r)$ should be zero or close to zero when r is at its maximum; (ii) back-calculation of $\rho(r)$ to $P(r)$ and $I(Q)$ should give curves similar to the starting $I(Q)$ and $P(r)$ curves; (iii) $\rho(r)$ should be stable and reproducible for different $I(Q)$ curves obtained under similar experimental conditions.

Determination of α-tocopherol and β-carotene content in LDL

At timed intervals for 2 h after the addition of Cu^{2+} to LDL at 37 °C, aliquots containing 0.5 mg of apoB were added to 1 ml of HPLC-grade hexane and 25 μl of 0.5 mM δ-tocopherol (12.5 nmol) as an internal standard, and assayed [19] in triplicate using normal-phase HPLC on a Beckman System Gold apparatus with a variable UV detector and a Nova-Pak Silica column (3.9 mm × 156 mm; 4 μm pore size).

Assay of lipid hydroperoxides and thiobarbituric acid-reactive substances (TBARS) in LDLs

The increase in the lipid peroxide content of LDL during oxidation was measured using the oxidative capacity of lipid peroxides, in which iodide is converted into iodine and this was measured photometrically at 365 nm using a colour reagent kit for cholesterol determinations (Merck Ltd., Poole, Dorset, U.K.) [20,21]. The TBARS colorimetric assay is based on the reaction of malondialdehyde with thiobarbituric acid [22] in the presence of 700 μM butylated hydroxytoluene and 100 μM EDTA. A 0.1 ml aliquot of malondialdehyde (0.122 M), which was freshly hydrolysed from 1,1,3,3-tetraethoxypropane (Sigma Chemical Company, Poole, Dorset, U.K.), was used as a standard. When 50 μl aliquots of LDL were removed for assay, 100 μl of 0.01 % butylated hydroxytoluene was added to stop oxidation, followed by additions of 400 μl of 10 % aqueous trichloroacetic acid and 400 μl of 0.75 % thiobarbituric acid, and incubation at 70 °C for 30 min. Assays were performed in triplicate.

The time course of conjugated-diene formation was monitored from the increase in the absorbance at 234 nm using a Beckman DU-65 spectrophotometer. In order to compare these changes with other products of oxidation, the conjugated-diene assay was conducted at 2 mg of apoB/ml and then diluted 20-fold to permit measurement of absorbance at concentrations where the Beer–Lambert law holds. The oxidized LDL was compared with diluted samples of native LDL at 20 min intervals.

Assay of LDL lipids by high-performance TLC (HPTLC)

Changes in the LDL lipids during oxidation were monitored using HPTLC [23]. At time points up to 44 h during LDL oxidation, lipids from 250 μg aliquots of apoB were extracted with 75 % efficiency [24]. The polar lipids were separated in a one-step procedure using a 25:25:25:10:9 (by vol.) mixture of methyl acetate, n-propanol, chloroform, methanol and 43 mM KCl in distilled water. 1,2-Dipalmitoylphosphatidylcholine, 1-palmitoyl-lysophosphatidylcholine and sphingomyelin (0.2–1.0 μg) were used as external standards (Sigma). The neutral lipids were likewise separated with a mixture of n-hexane, n-heptane, diethyl ether and acetic acid (63:18.5:18.5:1, by vol.). The external standards were triolein, cholesterol and cholesteryl linoleate (0.2–1.0 μg). Silica gel 60 chromatography plates (10 cm × 20 cm) (Merck) were prewashed in the solvent to be used for the lipid separation, and activated in an oven for 1 h at 110 °C. The samples and standards were applied with a Linomat (Camag) at the rate of 1 μl/5 s to the HPTLC plates (Merck). Lysophosphatidylcholine was quantified using about 100 μg of lipid (20 μg of apoB), phosphatidylcholine was quantified using about 10 μg of lipid (2 μg of apoB), and the neutral lipids were quantified using about 5 μg of lipid (1 μg of apoB). Plates used for phospholipid analyses were dried at room temperature and lightly sprayed with 1 mM toluidine naphthalene sulphuric acid/50 mM Tris, pH 7.4, every 10 min for 1 h. Plates used for neutral lipid analyses were dried in an oven at 110 °C for 10 min, immersed for 20 s in manganese chloride–sulphuric acid reagent (3.2 g of $MnCl_2$, 480 ml of methanol, 32 ml of concentrated H_2SO_4 and 480 ml of deionized water), placed horizontally on a paper towel to remove excess reagent, and dried in an oven at 110 °C for 35 min to char the lipid bands. Lipid quantification was performed with an automated TLC scanner with a Hg light source (Camag). The phospholipid plates were scanned for fluorescence at 222 nm. The neutral lipids plates were scanned for absorbance at 366 nm.

RESULTS AND DISCUSSION

X-ray Guinier analyses of native LDL

A total of 17 different native LDL samples were studied by synchrotron X-ray scattering at 4 °C, 15 °C and 40 °C in 22 dilution series between 0.9 and 10.9 mg of LDL protein/ml. At low Q values, Figure 1 illustrates how satisfactory linear Guinier fits in a $Q \cdot R_G$ range between 0.7 and 1.7 were obtained in a total of 187 LDL data acquisitions. Because of the larger X-ray R_G values and the need to retain a $Q \cdot R_G$ range similar to that used with neutron data [13], the fitted Q range is now reduced to 0.06–0.13 nm^{-1}, sometimes 0.10–0.13 nm^{-1} in place of the Q range of 0.08–0.19 nm^{-1} used for neutron analyses. Statistical errors of $\pm$0.2 nm in the R_G values at 10.9 mg/ml, rising to as much as $\pm$1 nm at 0.9 mg/ml, were encountered in the X-ray R_G analyses (results not shown), as it is necessary to work at low Q close to the main beam where background levels are increased. No radiation damage effects were observed in the 10 individual time-frames of each scattering curve. No temperature dependence

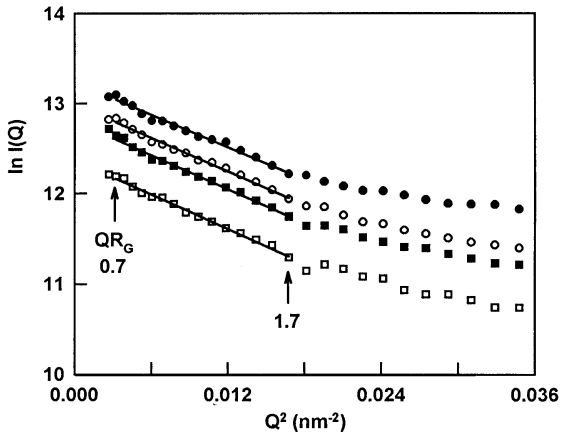

Figure 1 X-ray R_G and $I(0)$ Guinier plots for native LDL

A typical X-ray dilution series at LDL protein concentrations of 2.2, 4.4, 6.5 and 8.7 mg/ml (from bottom to top) for one LDL sample is shown, measured at 15 °C in PBS, using Station 8.2 at the SRS. The Guinier data were fitted in the Q range 0.08–0.12 nm^{-1}. The $I(Q)$ data points used for Guinier fits are denoted by straight lines, and the $Q \cdot R_G$ ranges are arrowed. A total of 17 LDL samples were studied in 22 dilution series.

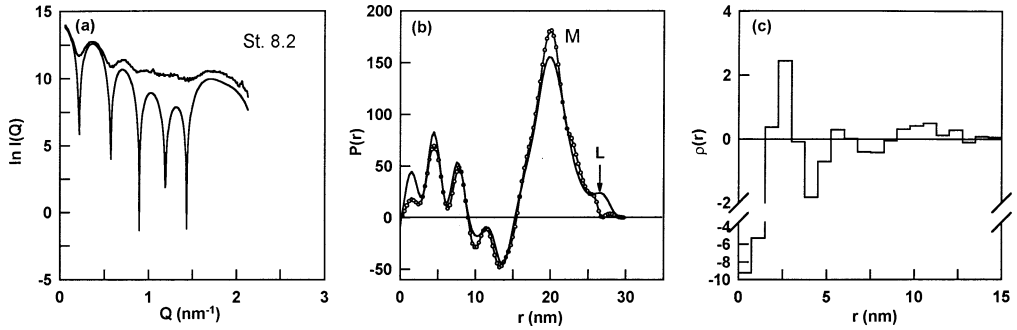

Figure 2 Full scattering curve $I(Q)$ for native LDL by X-ray solution scattering, with the corresponding distance distribution function $P(r)$ and radial electron-density function $\rho(r)$

The X-ray $\rho(r)$ curve was based on the $I(Q)$ curve at 4 °C extrapolated to zero concentration. (**a**) The starting $I(Q)$ curve (upper trace) is shown with the back-calculated $I(Q)$ curve obtained from the final $\rho(r)$ curve. The back-calculated curve is a theoretical representation that reproduces the main features of the observed curve, but takes no account of the polydispersity of the LDL sample that would otherwise fill in the sharp minima as shown. (**b**) The starting $P(r)$ curve (continuous line) is compared with the back-calculated $P(r)$ curve (●). The position of the maximum in $P(r)$ is denoted by M and the maximum dimension by L. (The units on the vertical scale are arbitrary.) (**c**) The final $\rho(r)$ curve is shown in 20 steps of 0.75 nm each (radius 15 nm).

in the R_G values was observed. Pronounced linear concentration dependences of the R_G and $I(0)/c$ values were observed (results not shown), similar to those observed with neutron scattering [13]. Extrapolation of the Guinier parameters to zero concentration by linear regression analyses was successful in all 22 LDL experiments. The extrapolated R_G values range between 12.1 and 16.0 nm at zero concentration, with a mean of 13.9 ± 1.0 nm. These agree with previously reported R_G ranges between 14 and 18 nm [10,25,26]. The range of extrapolated R_G and $I(0)/c$ values is consistent with the observation of ranges of values in neutron scattering [13], and indicate that LDLs are polydisperse in their structure. On account of this concentration dependence, oxidation studies of LDL structure are best performed at concentrations of 2 mg of LDL protein/ml.

X-ray-distance-distribution function and radial-electron-density function of native LDLs

The full X-ray-scattering curves were measured in a Q range of 0.08–2.46 nm^{-1}. A large submaximum is observed at Q of 1.77 nm^{-1} (Figure 2a), and this disappears on heating above 25–30 °C because of the lipid phase transition in LDLs [14]. Using this full Q range, the distance-distribution function $P(r)$ for each of the 187 LDL scattering curves, and for the 22 experiments extrapolated to zero concentration could be readily calculated using ITP. The phase transition is clearly visible in the $P(r)$ curves, where two positive submaxima at r of 4.5 nm and 7.5 nm and a negative one at r of 13.5 nm at 15 °C (Figure 2b) are transformed into broad features at 40 °C [26]. Comparison of the 22 extrapolated R_G and $I(0)/c$ values from the $P(r)$ curves showed that these agreed to within $5 \pm 9\%$ and $7 \pm 19\%$ respectively of the extrapolated Guinier analyses. Similar agreements were observed if the individual 187 $P(r)$ curves were used. The R_G values now ranged between 12.4 and 14.4 nm with a mean of 13.2 ± 0.7 nm. The $P(r)$ analyses were consistent with the Guinier analyses as required.

The $P(r)$ curve of LDL [25] corresponds to the ordered structure of the cholesteryl ester and triacylglycerol core of LDL between interparticle vectors r of 0 to 15 nm, while the maximum at r of 19.5 nm arises from the protein and phospholipid headgroups at the LDL surface. The best determination of L (the maximum dimension) from $P(r)$ gave values of 25–27 nm, although small oscillations in $P(r)$ made estimates difficult in this region (Figure 2b). The $\rho(r)$ curve at 4 °C (Figure 2c) corresponds to the ordered lipid core in LDL, where six positive and negative peaks are observed at r values of 0.8 nm, 3.0 nm, 4.5 nm, 6.0 nm, 8.3 nm and 11.3 nm. The latter two are less clear at 15 °C (Figures 3c and 3d). No significant concentration dependence of the $P(r)$ and $\rho(r)$ curves was seen for LDL protein concentrations between 1.3 and 6.3 mg/ml. The effect of polydispersity on LDL structures was analysed from X-ray $P(r)$ and $\rho(r)$ curves extra-

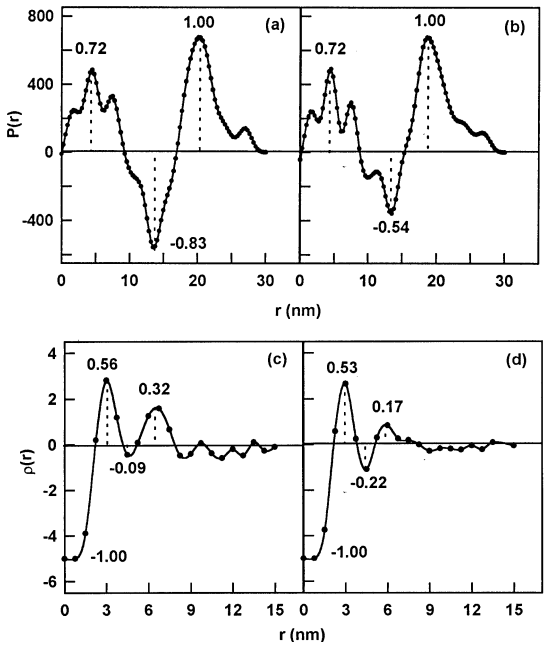

Figure 3 Comparison of the X-ray distance distribution function $P(r)$ and radial electron-density function $\rho(r)$ for LDL samples from two different donors

The scattering data were obtained during the same beamtime session. For each sample, eight $I(Q)$ curves were measured at 15 °C at four different LDL protein concentrations between 2.5 mg/ml and 10.0 mg/ml, extrapolated to zero concentration, and transformed using ITP-91 to the $P(r)$ curves (**a**,**b**) and using DECON-91 to the $\rho(r)$ curves (**c**,**d**). Those from the first donor are shown in (**a**,**c**), and those from the second donor in (**b**,**d**) (see text). The vertical scales in (**a**) and (**b**) are arbitrary.

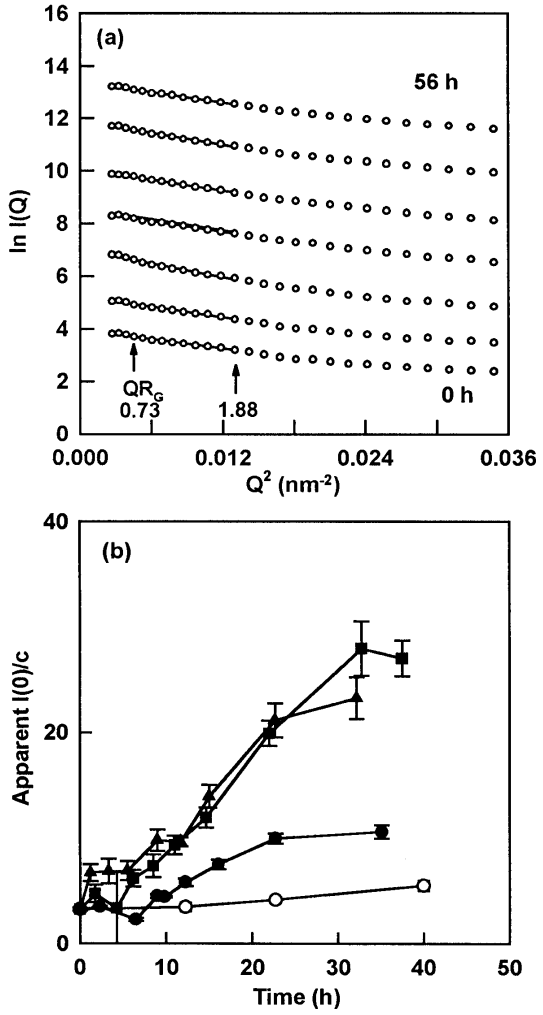

Figure 4 Synchrotron X-ray Guinier analyses for an oxidation time course of LDL

(**a**) Data were obtained at 2 mg/ml apoB at 0 h, 3 h, 13 h, 25 h, 31 h, 46 h and 56 h after the initiation of oxidation using 6.4 μmol of Cu^{2+}/g of apoB. Guinier plots were fitted in the Q range of 0.07–0.13 nm^{-1}, and the $Q \cdot R_G$ range is arrowed. The curves are displaced by 1.5 logarithmic units on the vertical axis for clarity. (**b**) The dependence of the Guinier $I(0)/c$ values with time of oxidation are shown for 6.4, 25.6 and 51.2 μmol Cu^{2+}/g of apoB (●, ■ and ▲ respectively). The control with no Cu^{2+} is denoted by ○. A total of 19 oxidation experiments were performed, of which three are shown here.

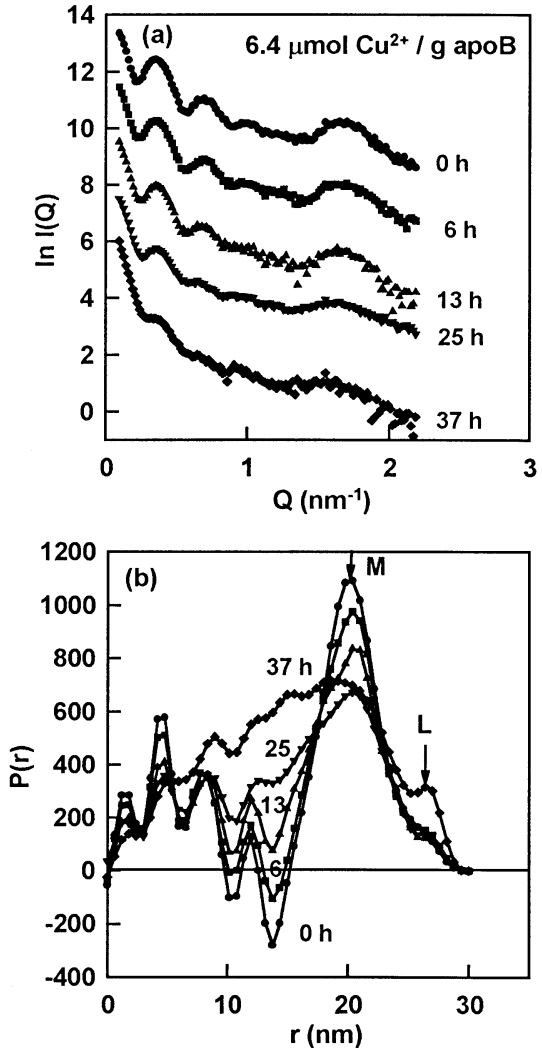

Figure 5 Time-dependence of the X-ray-scattering curves $I(Q)$ and distance distribution functions $P(r)$ on LDL oxidation

Results from one of a total of 19 oxidation experiments are shown here. (**a**) X-ray-scattering curves for LDL at an apoB concentration of 2 mg/ml and measured at 4 °C are shown at time points in an oxidation time course initiated with 6.4 μmol of Cu^{2+}/g of apoB. The curves are displaced by 2 logarithmic units on the vertical axis for clarity. (**b**) The corresponding $P(r)$ curves from (**a**) are shown. The position of the maximum in the $P(r)$ curves at r of 20.4 nm is denoted by M, and that of the maximum dimension by L in the same position as shown in Figure 2(b). The transformation of $I(Q)$ to $P(r)$ was based on 30 splines and an assumed maximum dimension of 30 nm for LDL.

polated to zero concentration for 14 different samples at 4 °C or 15 °C. The peak positions in $P(r)$ were well-conserved at 1.7 nm, 4.5 nm, 7.5 nm, 13.5 nm and 19–20 nm, but their intensities were not. If the intensity of the most intense peak in $P(r)$ at $r = 19$ nm was set as unity, that at $r = 4.5$ nm ranged between 0.46 and 0.77 and that at $r = 13.5$ nm ranged between -0.26 and -0.97 in the 14 LDL samples (Figures 3a and 3b). The corresponding $\rho(r)$ curves also exhibited large intensity fluctuations. The three peaks indicated in Figures 3(c) and 3(d) likewise ranged from 0.13 to 0.77, -0.09 to -0.35, and -0.02 to 0.51 in order of increasing r. Figures 3(a) and 3(c) correspond to LDL from a donor whose plasma cholesterol content was 4.0 mmol/l and triacylglycerol content was 0.67 mmol/l, while Figures 3(b) and 3(d) correspond to LDL from another donor who had high plasma lipid contents of 7.3 mmol/l cholesterol and 2.73 mmol/l triacylglycerol. In summary, these data indicate polydispersity in LDL structure and show that structural measurements of LDL oxidation are best made at 4 °C using the same sample in a given oxidation series.

X-ray Guinier analyses of the time course of LDL oxidation

Guinier R_G and $I(0)/c$ analyses for a typical oxidation time-course experiment with LDL are shown in Figure 4(a). Using 6.4 μmol of Cu^{2+}/g of apoB, significant increases in the R_G slopes of the Guinier plots in the accessible Q range that were seen by neutron scattering [11] in reflection of aggregate formation were not immediately evident. The scattering from these aggregates would occur at very low Q ranges that are encompassed by the

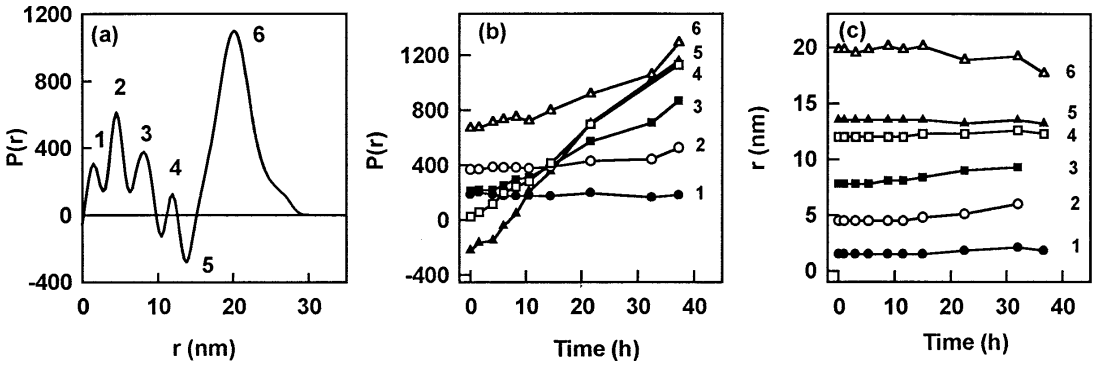

Figure 6 Time-dependence of changes in the internal structure of LDL from *P*(*r*) analysis during Cu^{2+}-initiated oxidation

(**a**) The numbering scheme of peaks 1 to 6 (●, ○, ■, □, ▲ and △ in that sequence) for five positive peaks 1–4 and 6 and one negative peak 5 that are consistently observed in the *P*(*r*) curves of LDL. The changes in these are summarized in (**b**) and (**c**). (**b**) The dependence of six peak intensities *P*(*r*) seen in Figure 5(b) on time after start of oxidation is shown for an LDL sample in which oxidation had been initiated with 51.2 μM Cu^{2+}. (**c**) The corresponding dependence of the six peak positions *r* during the same oxidation experiment is shown.

finite size of the beamstop, and neutron scattering is better for the study of LDL aggregation. Nonetheless, increases of 100–400 % in the apparent $I(0)/c$ values were detected (Figure 4b) in a typical LDL oxidation series based on three different Cu^{2+} concentrations (6.4, 25.6 and 51.2 μmol of Cu^{2+}/g of apoB) during 50 h of oxidation when compared with a control with no Cu^{2+} added. The larger the oxidative challenge of Cu^{2+}, the greater the increase in $I(0)/c$. These increases are comparable with those seen by neutrons, in which the apparent $I(0)/c$ increased by 53 %, 88 % and 110 % respectively under the same conditions (Figure 2b in [11]). The X-ray data therefore reflect the same processes that were observed by neutron scattering, and will correspond to a mixture of structures, including monomeric native LDL and aggregated oxidized LDL.

X-ray-distance-distribution function *P*(*r*) analyses of LDL oxidation

The full scattering curve $I(Q)$ of LDL at 4 °C in an oxidation time-course experiment initiated with 6.4 μmol of Cu^{2+}/g of apoB is shown in Figure 5(a). The 4–5 submaxima in the $I(Q)$ curve of native LDL gradually disappear during the 37 h time course of oxidation. This corresponds to the progressive loss of integrity of the LDL structure. Transformation of the $I(Q)$ curves into the $P(r)$ curves required the assumption of a maximum dimension for LDL. While Figures 2 and 3 had utilized 30 nm for this, and this had been reset as 60 nm for the neutron study of the aggregation of oxidized LDL [11], the present X-ray studies of LDL aggregation retained a value of 30 nm. The use of 60 nm resulted in unstable transforms of the $I(Q)$ curves to $P(r)$ curves. The use of 30 nm is justifiable on the basis of the neutron $P(r)$ curves which showed that 90–100 % of their intensities remained within $r = 0$–30 nm after 50 h of oxidation at all Cu^{2+} concentrations {Figure 4(a) of [5]}, and that the additional intensities between $r = 30$ and 60 nm after 50 h were at most 10 % of that between 0 and 30 nm with 6.4 μmol of Cu^{2+}/g of apoB {Figure 4(b) of [11]}. In other words, large changes in the $P(r)$ curve with the lowest Cu^{2+} concentration that arise early during the oxidation time course will correspond most closely to monomeric LDL and be the most significant.

The LDL $P(r)$ curves for which oxidation had been initiated with 6.4 μmol of Cu^{2+}/g of apoB are shown in Figure 5(b). The positive peaks 1, 2 and 3 at *r* values of 1.7, 4.5 and 7.5 nm in the $P(r)$ curves represent the cholesteryl ester core of LDL (Figure 6a) [14]. Peaks 1, 2 and 3 can be correlated with the large submaximum at Q of 1.77 nm^{-1} in $I(Q)$, as these all disappear during the lipid phase transition that occurs as LDL is heated from 4–15 °C to 37 °C. The negative peak 5 represents the hydrocarbon chains of phospholipid in the outer monolayer of LDL [14]. Peak 6 at $r = 20$ nm represents the protein and phospholipid head groups on the surface of LDL. The changes in the $P(r)$ curves during the LDL oxidation experiments were reproducible, as summarized in Figures 5(b), 6(b) and 6(c), and occurred more rapidly with increased Cu^{2+} concentrations.

The time course of structural change in the internal structure of LDL is represented in Figures 6(b) and 6(c), where this time oxidation had been initiated with 51.2 μmol of Cu^{2+}/g of apoB. The peak positions *r* in the $P(r)$ curves did not vary significantly during oxidation, but the peak intensities were altered. The magnitudes of the changes in peak intensity increased with Cu^{2+} concentration. The largest change in the $P(r)$ curves during oxidation occurred with peak 5 in Figure 6(b), and this is particularly dramatic in both Figures 5(b) and 6(b). Change in this peak is continuous and occurs shortly after the addition of Cu^{2+} to initiate oxidation, with no detectable lag phase. In Figure 6(b), peak 6 demonstrated a lag time of 12 h before change in this became apparent. Peak 6 demonstrated variable behaviour, as exemplified in Figures 5(b) and 6(b), as its intensity increased or decreased between different experiments. Further changes were observed in the lipid core of LDL, as evidenced by peak 3 in the $P(r)$ curves at an *r* value of 7.5 nm (Figure 5b). Peak 3 only altered significantly at Cu^{2+} concentrations of 25.6 and 51.2 μmol of Cu^{2+}/g of apoB, and a lag time of 8 h is apparent in Figure 6(b) before changes became noticeable.

Determination of the consumption of antioxidants in LDL

After depletion of ubiquinol-10, the antioxidants α-tocopherol and β-carotene become depleted during the first steps in the oxidative modification of LDL [27]. The concentration of α-tocopherol in native LDL, measured by HPLC in triplicate for each of three LDL samples, showed a mean value of 1.73 ± 0.76 mol/mol of apoB (1.73 ± 0.76 molecules of α-tocopherol per LDL particle). That for β-carotene measured by HPLC showed a mean value of 0.091 ± 0.026 mol/mol of apoB (0.091 ± 0.026 molecules of β-carotene per LDL particle). Both

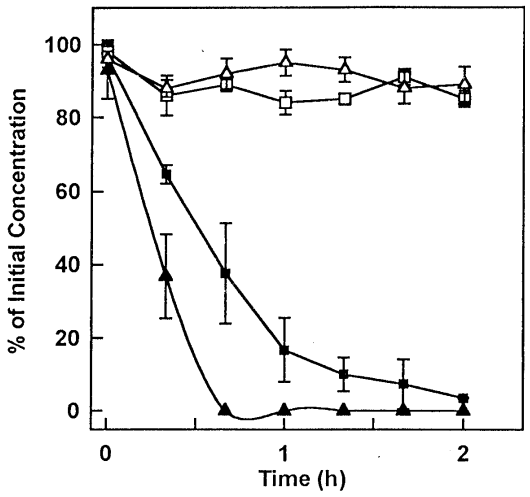

Figure 7 Loss of lipid antioxidants in LDL during oxidation with Cu^{2+}

Data are expressed as the percentage of the initial concentrations of α-tocopherol (▲) and β-carotene (■) as a function of time after Cu^{2+}-initiated oxidation was started using 6.4 μmol of Cu^{2+}/g of apoB. The open symbols correspond to the control without the addition of Cu^{2+}. Each point represents the mean ± S.D. from three LDL samples, where each sample was measured in triplicate.

determinations were lower than previously reported for Austrian subjects [28]. This may be due to the relatively small number of LDL samples analysed. Under the oxidation conditions used for our X-ray and neutron [11] work with 6.4 μmol of Cu^{2+}/g of apoB, α-tocopherol was found to be completely depleted after 40 min, while β-carotene was not depleted until after 80–120 min (Figure 7). The LDL samples become colourless. The use of 25.6 and 51.2 μmol of Cu^{2+}/g of apoB for depletion studies would result in shorter depletion times. These depletion times agree well with other data [29–31]. Under the conditions used in the X-ray experiments, it is seen that lipid peroxidation can start in LDL within the first 1–2 h after adding Cu^{2+}.

Formation of lipid hydroperoxides during LDL oxidation

LDL oxidation involves the conversion of polyunsaturated fatty acids in the LDL lipids into lipid hydroperoxides, the major initial products of lipid peroxidation. The formation of lipid hydroperoxide was studied in nine different LDL samples at three different Cu^{2+} concentrations. The initial quantities in the native LDL samples were 19 ± 7 nmol/mg of apoB. The maximum lipid hydroperoxide contents attained during LDL oxidation with 6.4, 25.6 and 51.2 μmol of Cu^{2+}/g of apoB were respectively 332 ± 57 nmol/mg of apoB (range 246–418 nmol/mg of apoB), 226 ± 47 nmol/mg of apoB (range 167–293 nmol/mg of apoB), and 138 ± 39 nmol/mg of apoB (range 94–189 nmol/mg of apoB). The time taken to reach the maximum concentration of lipid hydroperoxides was 12 h at all three different Cu^{2+} concentrations, after which the concentrations diminished. One such experiment is depicted in Figure 8(a). The higher the Cu^{2+} concentration used to initiate oxidation, the lower the maximum value of lipid hydroperoxide formed. This could be due to the more rapid breakdown of lipid hydroperoxides into aldehydes and ketones at higher Cu^{2+} concentrations. At 51.2 μmol of Cu^{2+}/g of apoB, it is likely that aldehydes were formed from lipid hydroperoxides nearly as rapidly as lipid hydroperoxides were being formed from polyunsaturated fatty acids.

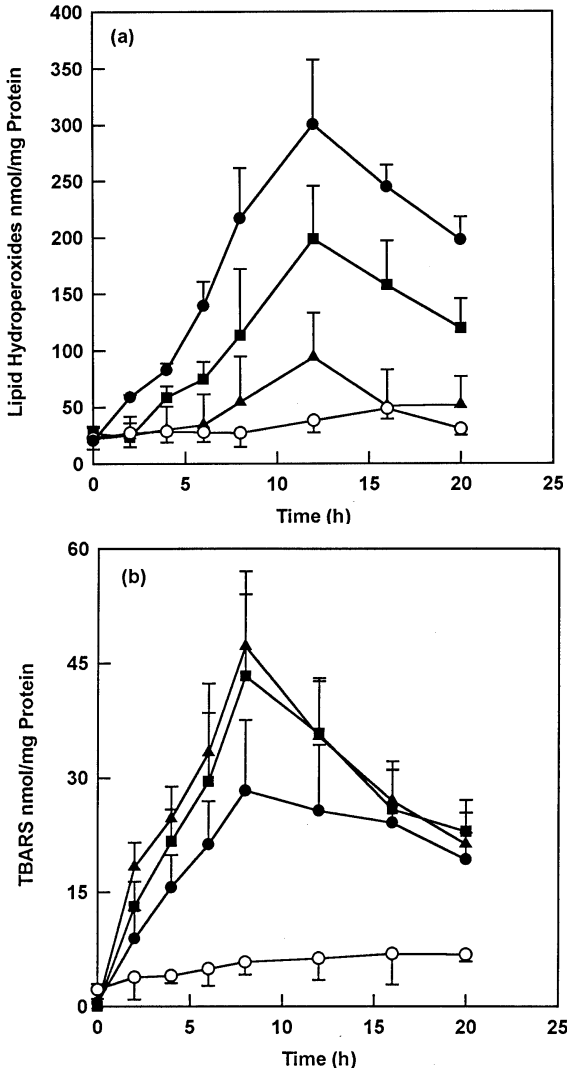

Figure 8 Time course of the development of lipid oxidation products in LDL

(**a**) Determinations of the mean content of lipid hydroperoxide in nmol/mg of apoB as a function of time after start of Cu^{2+}-initiated oxidation. (**b**) Determination of the mean formation of TBARS in nmol/mg of apoB is shown as a function of time after start of oxidation. In both (**a**) and (**b**), each point represents the mean ± S.D. of experiments with nine different LDL preparations, where the determination at each Cu^{2+} concentration for each LDL sample was made in triplicate. ○, no Cu^{2+} addition; ●, 6.4 μmol of Cu^{2+}/g of apoB; ■, 25.6 μmol of Cu^{2+}/g of apoB; ▲, 51.2 μmol of Cu^{2+}/g of apoB.

The peroxidation of polyunsaturated fatty acids in LDL is accompanied by an increase in UV absorbance at 234 nm [32]. This is due to the conversion of polyunsaturated fatty acids with isolated double bonds (18 : 2, 20 : 4) into fatty acid hydroperoxides with conjugated double bonds. The rate of oxidation measured by conjugated-diene formation was influenced by the concentration of LDL as well as the Cu^{2+} concentration. The maximal increase in the absorbance at 234 nm was similar for the different LDL preparations at a given Cu^{2+} concentration. There was a difference in the time taken to reach half-maximal absorbance, $t_{\frac{1}{2}}$, at different Cu^{2+} concentrations (results not shown). The mean (± S.D.) values of $t_{\frac{1}{2}}$ obtained with oxidations of LDL initiated with 6.4, 25.6 or 51.2 μmol of Cu^{2+}/g of apoB were 4.1 ± 0.8 h, 3.2 ± 0.3 h and 2.9 ± 0.7 h respectively. They

Table 1 HPTLC analysis of lipid contents in native LDL and in LDL during oxidation

Absolute quantities of lipids in LDL at 2 mg/ml apoB at the start and 44 h after initiation of oxidation with 6.4 μmol of Cu^{2+}/g of apoB. Values are expressed as mg/mg of apoB and are the means from three different LDL samples. Data for the control incubation without Cu^{2+} are summarized also.

	Mean literature values (mg/mg of apoB)	Initial HPTLC lipid composition (mg/mg of apoB)	Final HPTLC lipid composition (mg/mg of apoB)		Percentage change (%)	
			Control	6.4 μmol Cu^{2+}/g of apoB	Control	6.4 μmol Cu^{2+}/g of apoB
Polar lipids						
Sphingomyelin	0.24–0.28 [34,37]	0.33 ± 0.08	0.28 ± 0.04	0.15 ± 0.01	−15	−55
Phosphatidylcholine	0.62–0.66 [34,37]	0.60 ± 0.11	0.49 ± 0.05	0.23 ± 0.02	−18	−62
Lysophosphatidylcholine	0.07–0.074 [34,37]	0.04 ± 0.02	0.06 ± 0.01	0.37 ± 0.09	+50	+825
Others	0.023 [34,37]	Not determined				
Total phospholipid	1.00 ± 0.17	0.97 ± 0.07				
Neutral lipids						
Cholesterol	0.44 ± 0.03	0.48 ± 0.09	0.40 ± 0.08	0.31 ± 0.07	−17	−35
Triacylglycerol	0.26 ± 0.12	0.37 ± 0.08	0.30 ± 0.07	0.09 ± 0.05	−19	−76
Cholesteryl ester	1.90 ± 0.18	2.69 ± 0.25	2.22 ± 0.09	0.59 ± 0.11	−17	−78

show that conjugated dienes develop after the disappearance of antioxidants from LDL, and do so on a time scale similar to that of peroxidation (Figure 8a).

Formation of TBARS during LDL oxidation

Further LDL breakdown yields fragments such as ketones, alkanes and aldehydes [33]. The TBARS colorimetric assay was used to assess LDL oxidation by detection of the formation of malondialdehyde from polyunsaturated fatty acids with more than two double bonds, mainly arachidonic acid (Figure 8b). The mean quantity of TBARS in nine native LDL samples was 2.42 ± 1.92 nmol/mg of protein. The mean values of the maximum TBARS content obtained during LDL oxidation initiated with 6.4, 25.6 and 51.2 μmol of Cu^{2+}/g of apoB were respectively 28.4 ± 9.3 nmol/mg of apoB (range of 20.0–42.9 nmol/mg of apoB), 43.3 ± 10.7 nmol/mg of apoB (range 27.5–63.5 nmol/mg of apoB) and 47.2 ± 9.8 nmol/mg of apoB (range 33–50.3 nmol/mg of apoB). A maximum occurs at 8 h. The maximum amounts were 2–10-fold lower than those of lipid hydroperoxides formed, and depend on the Cu^{2+} concentration. As the TBARS assay quantifies malondialdehyde, and malondialdehyde is mainly derived from the catabolism of arachidonic acid, it is expected that lower levels of this will be formed when this is compared with levels of lipid hydroperoxides. On average, there are 150 molecules of arachidonic acid per LDL particle which give rise to malondialdehyde, compared with approx. 1300 polyunsaturated fatty acid molecules which give rise to lipid hydroperoxides [9].

The maximal formation of lipid hydroperoxides occurred at 12 h, while the maximal formation of malondialdehyde in the TBARS assay occurred at 8 h (Figure 8). It is concluded that arachidonic acid is preferentially oxidized to its breakdown product, malondialdehyde. This is supported by data that show, in the presence of Cu^{2+}, that the arachidonic acid in LDL is completely degraded within 3 h, while linoleic acid is not completely degraded until 12 h at LDL concentrations of 0.3 mg of protein/ml and 10 μM Cu^{2+} [9].

Changes in the lipid composition of LDL during oxidation

HPTLC determinations of the amounts of lipid in LDL and the changes in these which occur during oxidation were carried out. Comparison of the HPTLC data with earlier studies [9,34–39] shows that all are within error of each other except for those for cholesteryl esters (Table 1). This may arise from differences in the method of isolation of LDL from blood, which may lead to variations in the density profile of LDL. The density profile of LDL can have a profound effect on the lipid content of the sample [40].

The mean changes in the amounts of polar and neutral lipids in three different LDL samples over a 44 h time course when oxidation was initiated with 6.4 μmol of Cu^{2+}/g of apoB are summarized in Figure 9 and Table 1. Data for 25.6 and 51.2 μmol of Cu^{2+}/g of apoB yielded very similar results (not shown). For the polar lipids, Figure 9(a) shows the time course of changes in the amounts of sphingomyelin, phosphatidylcholine and lysophosphatidylcholine by HPTLC during oxidation. For the first 10–12 h, sphingomyelin levels remained constant, then were depleted to 45% after 44 h (Table 1). Phosphatidylcholine was continuously degraded with no observable lag time (less than 1 h), and this suggested that phosphatidylcholine was the initial primary site of oxidative modification. The reduction in phosphatidylcholine to 38% of its starting value is matched by an increase in the amount of lysophosphatidylcholine, indicating that phosphatidylcholine was hydrolysed to lysophosphatidylcholine. For the neutral lipids, Figure 9(b) shows that the amount of cholesterol remained unchanged for 10–12 h, and then slowly decreased. Triacylglycerols and cholesteryl esters also remained unmodified for the first 10 h, but then underwent a rapid decrease to levels of 25% (triacylglycerols) and 28% (cholesteryl esters) of their initial values after 28 h. Figure 9 indicates that oxidation is initiated at the periphery of the LDL particle, and moves on after 10–12 h to the other polar and neutral lipid classes.

Figure 9 and Table 1 are in good agreement with previous oxidation studies [39,41,42] on the individual lipid classes (Table 2). They show that LDL oxidation follows a clearly defined sequence. Only one previous study has reported the depletion of sphingomyelin and cholesteryl ester, in which the oxidation was carried out at 4 °C and not 37 °C, and is not therefore comparable with the present study [41]. The present data show that oxidative modification is initiated at an early stage in the outer monolayer of phospholipid in LDL through the hydrolysis of phosphatidylcholine. After 12 h, sphingomyelin is lost from the phospholipid monolayer, and at the same time the neutral lipids (cholesteryl

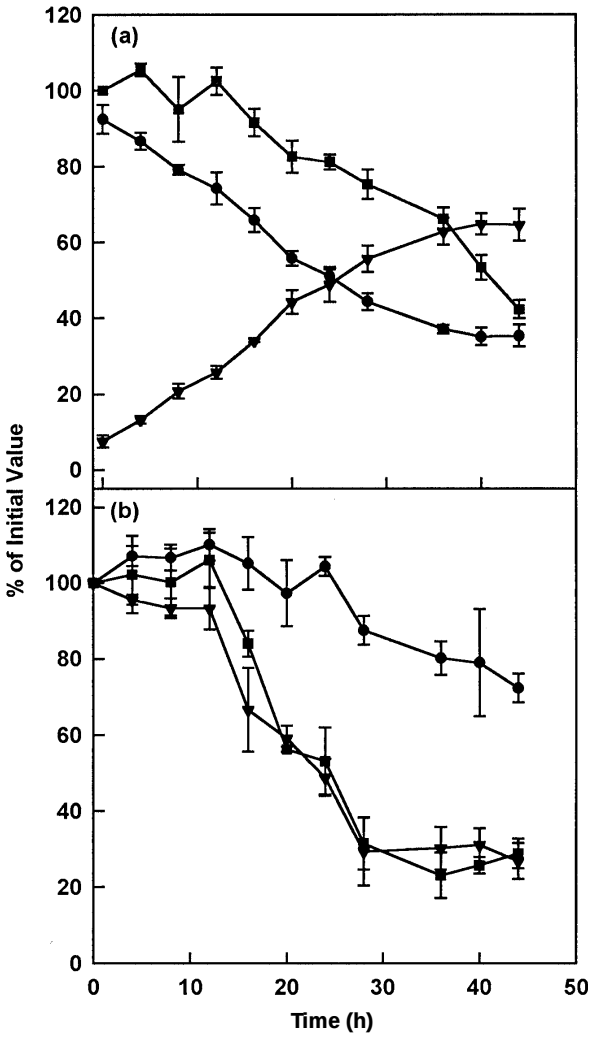

Figure 9 Determination of changes in the lipid composition of LDL by HPTLC analysis

Cu^{2+} oxidation for a 44 h time course was initiated with 6.4 μmol of Cu^{2+}/g of apoB. (**a**) Normalized amounts of three phospholipids during oxidation for phosphatidylcholine (●), sphingomyelin (■) and lysophosphatidylcholine (▼). (**b**) Normalized amounts of three neutral lipids during oxidation for cholesterol (●), cholesteryl ester (■) and triacylglycerol (▼). Each data point is the mean of triplicate determinations on three separate LDL samples, and they are shown as normalized values ± S.E.M. The starting values of the amounts of the six lipid classes were normalized to 100%, except for phosphatidylcholine and lysophosphatidylcholine for which the initial values were set to total 100%.

esters and triacylglycerols) are degraded in the LDL core. The cholesteryl ester and triacylglycerol lipids of the core are substantially modified after 28–30 h. The lipid class most resistant to oxidation appeared to be unesterified cholesterol. The observation of early oxidation products (lipid hydroperoxides and TBARS) within the first 12 h of oxidation appears to originate mainly from the phosphatidylcholine content of LDL.

Conclusions

Structure of LDL by synchrotron X-ray scattering

LDL particles are spherical with diameters in the range 19.7 nm to 27.0 nm. The present X-ray $P(r)$ data gave diameters between 25 and 27 nm, where the slight increase of up to 3 nm may result from the presence of a hydration shell around LDL that is detectable by X-rays, but which is ordinarily invisible by neutrons [10,43]. Electron microscopy gives a mean LDL diameter (±S.D.) of 23.6±3.2 nm, hydrodynamic studies give average LDL diameters of 22.9±2.4 nm, and neutron scattering gives a mean diameter of 23.1±1.2 nm [13]. The internal structure of LDL at 4 °C is best represented as two concentric shells of a core of triacylglycerol and cholesteryl ester, which is encased by a third concentric shell of apoB, phospholipid and cholesterol. Evidence for the location of apoB at the surface of LDL comes from: (i) the original X-ray-scattering analysis of LDL [14]; (ii) proteolysis and disulphide-bridge studies of apoB show that numerous segments are surface-exposed in LDL [44–47], and several surface-exposed heparin-binding sites occur along the length of the protein [48]; (iii) the core circumference of LDL increases linearly with increases in the length of 13 C-terminal apoB polypeptide fragments of different sizes [48,49]; (iv) protein is required to be on the LDL surface in order to satisfy packing constraints for the known amounts of protein and lipid in LDL and the surface area of LDL that is in contact with the aqueous phase [10,49,50]; (v) the use of monoclonal antibodies to map the course of apoB on the surface of LDL, which suggested that apoB surrounded LDL [51].

Table 2 Summary of previously reported values for lipid depletion in LDLs during oxidation, and the conditions under which these were achieved

Conditions: ref. [39], LDL at 0.15 mg/ml apoB was oxidized with 5 μM Cu^{2+} in PBS for 29 h at 37 °C; ref. [41], LDL at 0.1 mg/ml apoB was oxidized with 25 μM Cu^{2+} in M199 medium, pH 7.4, for 48 h at 4 °C; ref. [42], LDL at 0.1 mg/ml apoB was oxidized by endothelial cells for 20 h at 37 °C or with 5 μM Cu^{2+} in Ham's F-10 medium for 20 h at 37 °C.

LDL lipid component	Change during oxidation	Reference
Polar lipid		
Sphingomyelin	No significant change	[41]
Phosphatidylcholine	Depleted by 35–45%	[39,41]
Lysophosphatidylcholine	Increased by 250–300%	[39,41,42]
Neutral lipid		
Cholesterol	Depleted by 10%	[39,42]
Triacylglycerol	Depleted by 25–48%	[39,41,42]
Cholesteryl ester	Depleted by 52%	[41]

The variability of the X-ray-scattering curves of different LDL preparations in terms of Guinier and $P(r)$ analyses show that LDLs are polydisperse in their structures. This complements neutron data on LDLs which also indicate polydispersity [13]. Previous X-ray scattering on three LDL subfractions [52] at 10-fold higher LDL concentrations resulted in similar outer radii for the lipid core of 8.2–9.2 nm (errors of up to ±0.3 nm) and the LDL surface of 10.5–11.4 nm (errors of up to ±0.24 nm). This agrees with the conserved positions of the $P(r)$ and $\rho(r)$ peaks in the present study. Larger LDL particles contain typically 21% protein, 41% cholesteryl ester, 21% phospholipid, 11% cholesterol and 6% triacylglycerol, while smaller ones are more dense and contain typically 30% protein, 40% cholesteryl ester, 19% phospholipid, 9% cholesterol and 3% triacylglycerol [53]. Large volume changes in LDL will have a measurable effect on the R_G values [13], but have a small cube-root effect on the LDL radii, and this may account for the insensitivity of the positions of the $P(r)$ and $\rho(r)$ peaks to the LDL sample in use. However, variations in the packing of electron-dense and electron-light lipids within LDLs may cause the observed intensity changes in the $P(r)$ and $\rho(r)$ curves in the 14 different LDL samples that were

examined (Figure 3). Whether or not any correlation exists between these intensity changes and LDL lipid contents will require further study.

Synchrotron radiation makes possible the study of LDL in concentrations as low as 1 mg of apoB/ml. Data collection with 10 min run times have permitted both the detailed analyses of many native LDL samples and the kinetic study of the time course of structural changes in LDLs during oxidation. A complete oxidation series for LDL requires the use of the same LDL sample throughout as a reference, apoB concentrations of 2 mg/ml or less, and data collection at 4 °C. The present method offers advantages over older X-ray studies that quote typical X-ray accumulations not exceeding 5 h of data acquisition for LDL protein concentrations between 2 and 12 mg/ml [25], or 30 and 50 mg/ml [54].

Structural modifications to oxidized LDL by X-ray and neutron solution scattering

The present X-ray and neutron [11] time-course studies provide for the first time a description of the major structural events that take place in LDL during its oxidative breakdown using Cu^{2+}. Preliminary reports were published elsewhere [55,56]. These events are accompanied by complementary measurements on the composition of LDL during its oxidative modification under the same solution conditions. At the high concentrations of LDL in use, the oxidation rate was lower than in the more commonly used dilute solutions of LDL. The neutron oxidation data [11] show that LDLs undergo continuous aggregation into what is initially a non-covalently linked product. Neutron data show that oxidized LDLs largely retain their polydisperse spherical structure during the first 10 h of oxidation. Data from SDS/PAGE and the biological activity towards macrophages are consistent with the preservation of the integrity of the apoB polypeptide chain during this first 10 h period of Cu^{2+}-initiated oxidation [11]. It should be noted that local changes in apoB during this period are not ruled out by the scattering data, which evaluates structural events on a large scale. After 10 h of oxidation, the apoB structure begins to lose its integrity and LDL aggregation becomes sufficiently extensive to cause loss of the spherical LDL structure [13] and a reduction in uptake by macrophages [11]. After 30 h of oxidation, large disordered LDL aggregates are formed [11].

During oxidation, the negative peak 5 in the $P(r)$ curve changes first (and is accompanied by the neighbouring minor peak 4). Note that, as the X-ray $P(r)$ transformations require a spherical monomeric structure for LDL, the interpretations of the X-ray $P(r)$ curves are reasonably valid in the first 10 h of oxidation, and are less so after 10 h. Peak 5 corresponds to the ordered spherical shell of the fatty acid acyl chains of phospholipid near the surface of LDL. This peak is negative in intensity as the CH_2 hydrocarbon group in LDL is less electron dense than water molecules. One explanation of the increase in intensity of peak 5 is that this may result from a significant incorporation of oxygen within unsaturated acyl chains at the sites of hydrogen abstraction. As about half the fatty acids in LDL are polyunsaturated, large amounts of hydroperoxides will be formed during oxidation. During oxidation, the double bonds in the fatty acid chains will become oxidized. These chains will incorporate oxygen at sites where abstraction of a hydrogen atom results in the formation of an alkyl radical. Such a substantial oxygen uptake in LDL has been reported; after oxidation had been initiated with 2 μM $CuCl_2$, a solution of 0.25 mg of LDL protein/ml had taken up 100 μM oxygen by 3 h [57]. This uptake would increase the electron density of the acyl chains and cause the intensity of peak 5 to increase. Another explanation of the increase in peak 5 is that this corresponds to structural disorder in the phospholipid monolayer at the surface of LDL. The replacement of the two-chain phosphatidylcholine molecules in this monolayer by mono-chain lysophosphatidylcholine molecules may destabilize the structure of this outer lipid monolayer. Indeed, after 44 h of oxidation, more lysophosphatidylcholine is present than phosphatidylcholine (Table 1). By either or both of these hypotheses, the annular shell of phospholipid hydrocarbon in native LDL has become disorganized into non-spherical structures with the growth of the lysophosphatidylcholine component in oxidized LDL.

The second set of changes in the X-ray $P(r)$ curves involves peaks 6 and 3. These are gradual in the first 10 h of oxidation, but thereafter become more noticeable. Peak 6 corresponds to the phospholipid headgroups and apoB on the surface of LDL, and peak 3 corresponds to structural features of the neutral lipid core. After 10 h of oxidation, the increasing disorganization of the acyl chains in the outer phospholipid monolayer of LDL appears to influence the remainder of the LDL structure. SDS/PAGE shows that this is when apoB loses its structural integrity [11], and implies that LDL would start to lose its ability to maintain a spherical structure. This would account for the changes in peak 6 after 10–12 h. HPTLC analysis (Figure 9) shows that the later stages of oxidation involve the oxidative modification of all the lipid classes in LDL, including the core lipids of cholesteryl esters and triacylglycerols. The changes in peak 3 after 10–12 h show that the ordered structure of the lipid core begins to change to a less well defined spherical structure. The maximal uptake of oxidized LDL by macrophages occurs at 10 h after initiation of oxidation [11], a stage where the core lipids have not been extensively modified. It is not likely that oxidative damage to the core lipids is significant for macrophage uptake under our conditions. The changes in peak 3 are thus best explained in terms of the development of larger aggregates of oxidized LDL, as seen by neutron scattering.

Changes in the composition of LDL during oxidation

After depletion of the antioxidants α-tocopherol and β-carotene within the first 2 h of the Cu^{2+}-initiated oxidations in the present study (Figure 7), the early stages of LDL oxidation, up to 8–10 h, were mainly confined to the surface phospholipid monolayer of LDL, where the decrease in phosphatidylcholine is matched by a similar increase in lysophosphatidylcholine (Figure 9). The HPTLC analyses show that, after a lag time of approx. 12 h, other lipid classes in LDL become oxidatively modified. This leads to an overall picture of LDL oxidation that is initiated at the surface monolayer of phospholipid, and is progressively extended to the modification of the lipids in the LDL core. It has been reported that cholesteryl ester hydroperoxides appear in the early stages of oxidation [57], but this accounts for only a small percentage of the total cholesteryl ester content and is not therefore detectable by HPTLC. Arachidonic acid was found to be more prone to oxidation than other polyunsaturated fatty acids, and evidence for this was shown by the maximum reached by the TBARS assay (Figure 8b) before that reached by the lipid hydroperoxide assay (Figure 8a). This indicates that the early stages of phosphatidylcholine oxidation are characterized by the oxidation of polyunsaturated fatty acids (arachidonic acid), which, because of their greater degree of unsaturation, are more susceptible to oxidation than other polyunsaturated fatty acids such as linoleic acid.

In conclusion, both the X-ray scattering and compositional analyses show that the initial stages of Cu^{2+}-initiated oxidation

are characterized mainly by the structural and biochemical modification of surface phosphatidylcholine and phospholipids containing arachidonic acid. Later stages of oxidation involve the protein and neutral lipid contents of LDL. Neutron scattering shows that these result in the eventual destruction of the spherical LDL particle to form large aggregates [11].

We thank the Science and Engineering Research Council and SmithKline and Beecham plc for a CASE studentship to D.F.M., the Wellcome Trust and the SmithKline (1982) Foundation for support, and Dr. O. Glatter for the PDH, ITP and DECON programs. We thank Dr. W. Bras for excellent instrumental support at the SRS facility, and Mr. T. Bunce for technical support.

REFERENCES

1 Durrington, P. N. (1991) Hyperlipidaemia: Diagnosis and Management, Wright, London
2 Rudel, L. L., Parks, J. S., Johnson, F. L. and Babiak, J. (1986) J. Lipid Res. **27**, 465–472
3 Krauss, R. M. and Blanche, P. J. (1992) Curr. Opin. Lipidol. **3**, 377–383
4 Goldstein, J. L. and Brown, M. S. (1983) in The Metabolic Basis of Inherited Disease (Stanbury, J. B. et al., eds.), pp. 672–712, McGraw-Hill, New York
5 Steinberg, D. and Witztum, J. L. (1990) J. Am. Med. Assoc. **264**, 3047–3052
6 Witztum, J. L. and Steinberg, D. (1991) J. Clin. Invest. **88**, 1785–1792
7 Rice-Evans, C. and Bruckdorfer, K. R. (1992) in Molecular Aspects of Medicine (Baum, H., ed.), vol. 13, pp. 1–112, Pergamon Press, Oxford
8 Esterbauer, H., Gebicki, J., Puhl, H. and Jürgens, G. (1992) Free Rad. Biol. Med. **13**, 341–390
9 Esterbauer, H., Dieber-Rotheneder, M., Waeg, G., Striegl, G. and Jürgens, G. (1990) Chem. Res. Toxicol. **3**, 77–92
10 Bellamy, M. F., Nealis, A. S., Aitken, J. W., Bruckdorfer, K. R. and Perkins, S. J. (1989) Eur. J. Biochem. **183**, 321–329
11 Meyer, D. F., Mayans, M. O., Groot, P. H. E., Suckling, K. E., Bruckdorfer, K. R. and Perkins, S. J. (1995) Biochem. J. **310**, 417–426
12 Perkins, S. J. (1994) in Methods in Molecular Biology, vol. 22 (Jones, C., Mulloy, B. and Thomas, A. H., eds.), pp. 39–60, Humana Press Inc., New Jersey
13 Meyer, D. F., Nealis, A. S., Bruckdorfer, K. R. and Perkins, S. J. (1995) Biochem. J. **310**, 407–415
14 Laggner, P. and Müller, K. W. (1978) Q. Rev. Biophys. **11**, 371–425
15 Towns-Andrews, E., Berry, A., Bordas, J., Mant, G. R., Murray, P. K., Roberts, K., Sumner, I., Worgan, J. S., Lewis, R. and Gabriel, A. (1989) Rev. Sci. Instrum. **60**, 2346–2349
16 Worgan, J. S., Lewis, R., Fore, N. S., Sumner, I. L., Berry, A., Parker, B., D'Annunzio, F., Martin-Fernandez, M. L., Towns-Andrews, E., Harries, J. E., Mant, G. R., Diakun, G. P. and Bordas, J. (1990) Nuclear Instruments Methods Physics Res. **A291**, 447–454
17 Glatter, O. and Kratky, O. (1982) Small-angle X-ray Scattering, Academic Press, New York
18 Müller, K. and Glatter, O. (1982) Makromol. Chem. **183**, 465–479
19 Rice-Evans, C., Diplock, A. T. and Symons, M. C. R. (1991) in Techniques in Free Radical Research, pp. 185–190, Elsevier, Amsterdam
20 El-Saadani, M., Esterbauer, H., El-Sayed, M., Goher, M., Nassar, A. Y. and Jürgens, G. (1989) J. Lipid Res. **30**, 626–630
21 Thomas, S. M., Jessup, W., Gebicki, J. M. and Dean, R. T. (1989) Anal. Biochem. **176**, 353–359
22 Gutteridge, J. M. C. and Quinlan, G. J. (1983) J. Appl. Biochem. **5**, 293–299
23 Tew, D. G., Southan, C., Rice, S. Q. J., Lawrence, M. P., Li, H., Saul, H. F., Moores, K., Gloger, I. S. and MacPhee, C. H. (1996) Arteriosclerosis Thromb. Vasc. Biol. **16**, 591–599
24 Bligh, E. G. and Dyer, W. J. (1959) Can. J. Biochem. Physiol. **37**, 911–917
25 Laggner, P., Degovics, G., Müller, K. W., Glatter, O., Kratky, O., Kostner, G. and Holasek, A. (1977) Hoppe-Seyler's Z. Physiol. Chem. **358**, 771–778
26 Müller, K., Laggner, P., Glatter, O. and Kostner, G. (1978) Eur. J. Biochem. **82**, 73–90
27 Jessup, S., Rankin, M., De-Whalley, C. V., Hoult, R. S., Scott, J. and Leake, D. S. (1990) Biochem. J. **265**, 399–405
28 Esterbauer, H., Puhl, H., Dieber-Rotheneder, M., Waeg, G. and Rabl, H. (1991) Annals Med. **23**, 573–581
29 Kalyanaraman, B., Antholine, W. E. and Parthasarathy, S. (1990) Biochim. Biophys. Acta **1035**, 286–292
30 Sato, K., Niki, E. and Shimasaki, H. (1990) Arch. Biochem. Biophys. **279**, 402–405
31 Bowry, V. W., Ingold, K. U. and Stocker, R. (1992) Biochem. J. **288**, 341–344
32 Esterbauer, H., Striegl, G., Puhl, H. and Rotheneder, M. (1989) Free Rad. Res. Commun. **6**, 67–75
33 Esterbauer, H., Jürgens, G., Quehenberger, O. and Koller, E. (1987) J. Lipid Res. **28**, 495–509
34 Yla-Herttuala, S., Jaakkola, O., Ehnholm, C., Tikkanen, M. J., Solakivi, T., Sarkioja, T. and Nikkari, T. (1988) J. Lipid Res. **29**, 563–572
35 Hoff, H. F. and Gaubatz, J. W. (1982) Atherosclerosis **42**, 273–297
36 Sattler, W., Kostner, G. M., Waeg, G. and Esterbauer, H. (1991) Biochim. Biophys. Acta **1081**, 65–74
37 Laggner, P., Kostner, G. M., Rakusch, U. and Worcester, D. (1981) J. Biol. Chem. **256**, 11832–11839
38 Steinbrecher, U. P. (1987) J. Biol. Chem. **262**, 3603–3608
39 Barenghi, L., Bradamante, S., Giudici, G. A. and Vergani, C. (1990) Free Rad. Res. Commun. **8**, 175–183
40 de Graff, J., Hak-Lemmers, H. L. M., Hectors, M. P. C., Demacker, P. N. M., Hendricks, J. C. M. and Stalenhoef, A. F. H. (1991) Arteriosclerosis Thromb. **11**, 298–306
41 van Hinsbergh, V. W. M., Scheffer, M., Havekes, L. and Kempen, H. J. M. (1986) Biochim. Biophys. Acta **878**, 49–64
42 Steinbrecher, U. P., Parthasarathy, S., Leake, D. S., Witzum, J. L. and Steinberg, D. (1984) Proc. Natl. Acad. Sci. U.S.A. **81**, 3883–3887
43 Perkins, S. J. (1986) Eur. J. Biochem. **157**, 169–180
44 Chen, G. C., Zhu, S., Hardman, D. A., Schilling, J. W., Lau, K. and Kane, J. P. (1989) J. Biol. Chem. **264**, 14369–14375
45 Chen, G. C., Hardman, D. A., Hamilton, R. L., Mendel, C. M., Schilling, J. W., Zhu, S., Lau, K., Wong, J. S. and Kane, J. P. (1989) Biochemistry **28**, 2477–2484
46 Yang, C., Gu, Z. W., Weng, S., Kim, T. W., Chen, S. H., Pownall, H. J., Sharp, P. M., Liu, S. W., Li, W. H., Gotto, Jr., A. M. and Chen, L. (1989) Arteriosclerosis **9**, 96–108
47 Yang, C., Kim, T. W., Weng, S., Lee, B., Yang, M. and Gotto, Jr., A. M. (1990) Proc. Natl. Acad. Sci. U.S.A. **87**, 5523–5527
48 Chan, L. (1992) J. Biol. Chem. **267**, 25621–25624
49 Spring, D. J., Chen-Liu, L. W., Chatterton, J. E., Elovson, J. and Schumaker, V. N. (1992) J. Biol. Chem. **267**, 14839–14845
50 Shen, B. W., Scanu, A. M. and Kézdy, F. J. (1977) Proc. Natl. Acad. Sci. U.S.A. **74**, 837–841
51 Chatterton, J. E., Phillips, M. L., Curtiss, L. K., Milne, R. W., Marcel, Y. L. and Schumaker, V. N. (1991) J. Biol. Chem. **266**, 5955–5962
52 Baumstark, M. W., Kreutz, W., Berg, A., Frey, I. and Keul, J. (1990) Biochim. Biophys. Acta **1037**, 48–57
53 Chapman, M. J., Laplaud, P. M., Luc, G., Forgez, P., Bruckert, E., Goulinet, S. and Lagrange, D. (1988) J. Lipid Res. **29**, 442–458
54 Atkinson, D., Deckelbaum, R. J., Small, D. M. and Shipley, G. G. (1977) Proc. Natl. Acad. Sci. U.S.A. **74**, 1042–1046
55 Meyer, D. F., Nealis, A. S., Bruckdorfer, K. R. and Perkins, S. J. (1993) J. Physique IV **3**, 257–260
56 Meyer, D. F., Nealis, A. S., Bruckdorfer, K. R. and Perkins, S. J. (1993) Biochem. Soc. Trans. **21**, 139S
57 Noguchi, N., Gotoh, N. and Niki, E. (1993) Biochim. Biophys. Acta **1168**, 348–357

Received 7 February 1996/24 May 1996; accepted 7 June 1996